UNIVERSITY OF CALIFORNIA,
IRVINE

Thermal metrology development and thermal conductance limits of low-dimensional nanostructures

THESIS

Submitted in partial satisfaction of the requirements
for the degree of

MASTER OF SCIENCE

In Chemical and Biochemical Engineering

by

Majed S. Madani

Thesis Committee:
Professor Jaeho Lee, Chair
Professor Alon Gorodetsky
Professor Allon Hochbaum

2017

TABLE OF CONTENTS

LIST OF FIGURES

ACKNOWLEDGEMENT

I would like to offer my sincerest gratitude to Professor Jaeho Lee who has patiently supported me throughout my studies as a Master's student. I am very thankful that Professor Lee has offered me the chance to join his lab. Working in Nano Thermal Energy Research (NTER) lab, and under Professor Lee's guidance, I have learned a lot about nanoscale heat transfer. My interest has grown as I progressed over the last year which has sparked my desire to further continue working on this field for my graduate studies. I was also fortunate to be one of the founding students of this new research group, which allowed me to establish my own experimental research from scratch.

I also want to thank my committee members, Professor Allon Hochbaum for his collaboration and guidance in pushing forward this project, and Professor Alon Gorodetsky for his collaboration with potential future projects.

I cannot forget the countless of hours that I have spent with my colleagues in the lab and the challenges we have faced together as we progressed. I would not have had better labmates other than NTER members who encouraged and supported me through many ups and downs. Not to mention, my family and friends who are still supporting and encouraging me to pursue my graduate degrees even at the expense of being far away from them.

I dedicate this work to all whom I have had worked with, and those who guided me throughout my studies.

ABSTRACT OF THE THESIS

Thermal metrology development and thermal conductance limits of low-dimensional nanostructures

By

Majed S. Madani

Master of Science in Chemical and Biochemical Engineering
University of California, Irvine, 2017
Professor Jaeho Lee, Chair

With the advancement of synthetic nanostructures, more attention has been directed toward probing low-dimensional transport phenomena. Recently, multiple techniques have been established for thermal transport measurements at the nanoscale domain. Sensitivity analysis however remains an experimental challenge for both high and low conductance materials. Achieving precise thermometry remains an obstacle due to influence of thermal contact resistance particularly at cryogenic temperatures where boundary scattering is more dominant. The contribution of radiation heat exchange is also a concern which is more critical at higher temperatures exceeding 800 K. Here we report the limitations of thermal conductance measurements in silicon nanowires and other common nanostructures by evaluating the thermal conductance limit according to the geometrical characteristics and temperature. This study will illustrate experimental results of thermal conductivity measurements using a suspended micro-device with built-in resistive thermometers and report the measurement limitations computationally for probing thermal transport in 1-D and 2-D nanostructures.

Chapter 1 Introduction

Heat transfer problems at the macroscale are based on solving conservation and constitutive equations. The formulation of Fourier's law of heat conduction in 1822 [1] established the foundation of studying heat conduction at the macroscale level. Fourier's law can be expressed as

$$q = -k\nabla T \tag{1}$$

where q is the local heat flux, k is the temperature dependent thermal conductivity of the material, and ∇T is the temperature gradient. In nanostructures, such as nanowires, nanotubes, and thin films, Fourier law is not applicable because the length scale associated with the energy carriers is comparable to or larger than the characteristic length of the nanostructure [2]. With the emergence of nanoscale heat transfer during the past two decades, more attention has been directed toward finding applicable methods to probe thermal properties of nanostructures. [3] Significant progress has been made towards understanding thermal transport processes of low dimensional nanostructures, including silicon [4,7,9,10], carbon based materials, [11], and multiple two-dimensional materials [10]. The growing interest in synthetic nanostructures for numerous applications has led researchers to develop measurement techniques probing thermal properties in one-dimensional (1D) and two-dimensional (2D) nanostructures [3,5]
With the ongoing development of measurement techniques of thermal conductance of nanostructures, addressing experimental limitations such as boundary resistance and influence of radiation are inevitable. Thus, to have an accurate estimation of reported thermal conductance, it is essential to quantify the lower and upper limits of conductance for each corresponding material.

Modeling thermal transport in nanostructures

In contrast to bulk thermal conduction, analyzing thermal conduction in nanostructure requires more rigorous thermal conductivity modeling. In this work, we model thermal conductivity based on Boltzmann Transport Equation (BTE) [13-18]. We show the derivation of BTE to model thermal conductivity of silicon nanostructure. BTE considers phonons as particles with energy and momentum. BTE model uses the distribution function $f\ (x, p, t)$, where x, p, t represent geometric space, momentum space, and time, respectively. The distribution function is used to describe the conservations of the number of particles. Equation (1) shows the general form of the BTE.

$$\left(\frac{\partial f}{\partial t}\right)_{scattering} = \frac{\partial f}{\partial t} + v \cdot \nabla_x f + \frac{F}{m} \cdot \nabla_p \tag{2}$$

where $\left(\frac{\partial f}{\partial t}\right)_{scattering}$ represent the time rate of change of the number of particles due to scattering, $\frac{\partial f}{\partial t}$ represents the total time rate of change of number of particles, $v \cdot \nabla_x$ represent particle diffusion in geometric space to phonon group velocity (v), and $\frac{F}{m} \cdot \nabla_p f$ represents the acceleration in momentum space to external forces. With no external forces and assuming steady-state, the first

and third terms of the right-hand side of Eq (2) can be dropped. $\left(\frac{\partial f}{\partial t}\right)_{scattering}$ can be replaced by the departure of the distribution function from equilibrium divided by the relaxation time. Therefore, the equation simplifies to

$$v \cdot \nabla_x f = -\frac{f - f_{eq}}{\tau} \quad (3)$$

following Bose-Einstein statistical distribution, the number of phonons for a given frequency, ω and at an equilibrium temperature T, f_{eq} is expressed as

$$f_{eq} = \frac{1}{exp\left(\frac{\hbar\omega}{k_B T}\right) - 1} \quad (4)$$

We also assume a small deviation from equilibrium which simplifies the left hand of equation (3)

$$\nabla_x f \approx \nabla_x f_{eq} = \frac{\partial f_{eq}}{\partial T} \nabla_x T \quad (5)$$

This gives us a reduced equation of BTE in the form of

$$f = f_{eq} - v\tau \cdot \frac{\partial f_{eq}}{\partial T} \nabla_x T \quad (6)$$

The heat flux can be expressed as the product of group velocity and energy density integrated over all phonon frequencies

$$q_x = \int v_x \, \hbar\omega D_p f \, d\omega \quad (7)$$

from BTE expression, the heat flux equation becomes

$$q = \int -\frac{1}{3} v_g^2 \tau \hbar\omega \frac{\partial f_{eq}}{\partial T} D_p d\omega \frac{\partial T}{\partial x} \quad (8)$$

The $\frac{1}{3}$ term is associated with isotropic case in which the group velocity is the same in the x, y and z directions, or $v_x^2 = \frac{v_g^2}{3}$

According to Fourier Law for heat conduction, the thermal conductivity is expressed as

$$k = \int \frac{1}{3} v_g^2 \tau \hbar\omega \frac{\partial f_{eq}}{\partial T} D_p d\omega \quad (9)$$

Phonon heat capacity is obtained by differentiating internal energy with respect to temperature. From the heat capacity equation, we obtain to simple kinetic theory model for thermal conductivity as shown in equation (12)

$$C = D_p \hbar\omega = \frac{\partial f_{eq}}{\partial T} = D_p k_B \frac{\left(\frac{\hbar\omega}{k_b T}\right)^2 exp\,(\frac{\hbar\omega}{k_b T})}{(exp\left(\frac{\hbar\omega}{k_b T}\right)-1)^2} \quad (10)$$

$$C = \frac{\partial u}{\partial T} = \sum_{polar.} \int \hbar\omega \frac{\partial f_{eq}}{\partial T} D_p \, d\omega \quad (11)$$

A simple kinetic theory model for thermal conductivity can be expressed as

$$k = \frac{1}{3} C v_g \Lambda \quad (12)$$

where Λ is the phonon mean free path and is equal to 40. 9 nm for silicon. v_g is the phonon group velocity and is approximately 6400 m/s. [18]

Relaxation time approximation

Computing thermal conductivity at the nanoscale domain requires information about heat capacity, group velocity, and relaxation time. It has been shown that the thermal conductivity is expected to reduce due to increased boundary scattering and phonon dispersion modification [19,20]. Relaxation time accounts for size effect in low-dimensional materials by estimating phonon scattering events. This phenomenon can be modeled by Matthiessen's rule. For crystalline materials, the phonon relaxation time can be modeled as

$$\tau^{-1} = \tau_U^{-1} + \tau_B^{-1} + \tau_D^{-1} \quad (13)$$

where τ_U^{-1} is the relaxation time accounting for Umklapp (phonon-phonon) scattering, τ_B^{-1} is the relaxation time accounting for boundary scattering, and τ_D^{-1} is the relaxation time accounting for defects scattering. The relaxation time due to Umklapp scattering can be expressed as

$$\tau_U = AT\omega^2 \, exp\left(-\frac{B}{T}\right) \quad (14)$$

where A=1.4 x 10^{-19} s/K and B=152 K are fitting parameters [21]. At high temperatures, the Umklapp scattering mean free path term begins to scale inversely with temperature, which corresponds to increasing population of phonons and increasing phonon-phonon scattering events. The relaxation time due to boundary scattering can be expressed as

$$\tau_B = \frac{L}{2v_g} \quad (15)$$

where L is the characteristic length of the nanostructure, and v_g is the group velocity. Finally, the relaxation time due to defect scattering takes the form of

$$\tau_D = D\omega^4 \quad (16)$$

where D= 1.32 x 10^{-45} s^3 which is mainly dependent on the isotope concentration for nearly pure silicon. [21]

Chapter 2 Microfabricated device and sample preparation

Conventional techniques used for measuring bulk thermal conductivity cannot be used for 1D nanostructures due to the small size of the sample which requires fabricating microscale devices. In this section, we will introduce one measurement technique pioneered by Li shi et al.

The microdevice is a suspended structure consisting of two adjacent 25 μm x 35 μm low stress SiNx membranes with five 400 μm long, 2 μm wide and 0.3 μm thick SiNx beams.
A platinum resistive thermometer (PRT), which also serves as a heater is designed on each membrane. The platinum coil is 30 nm thick and 800 nm wide and is connected to a 300 μm x 300 μm Pt bonding pads on the substrate via the Pt leads on the SiNx beams that hold the suspended membranes. Another 1.5 μm wide Pt electrode is designed on each membrane which is used to provide electrical contact to the suspended sample across the gap [5].

Silicon nanowire synthesis and preparation

In this work, Silicon nanowires was fabricated by metal-assisted chemical etching. The procedure starts with depositing metal by electroless deposition or galvanic exchange. The following step is the etching process where it is achieved in a solution of HF. In this method, we use silver nitrate. When silver is used, silver ions in the proximity of the silicon surface captures electrons from the valance band of silicon. Meanwhile holes are generated in the silicon valance band when the silver ion Is reduced to silver nuclei. Deposition of the silver nuclei facilitates the formation of silicon dioxide underneath the silver nanoparticle. Silicon dioxide is etched away by hydroflouric acid This leads the nanoparticles to sink into the silicon surface forming silicon nanowires as shown in Figure 1 The reactions taking place on the surface of Silicon are as follows [22].

$$Ag^+ + e^- \rightarrow Ag^0(0)$$

$$Si(s) + 2H_2O \rightarrow SiO_2 + 4H^+ + 4e^-$$

$$SiO_2(s) + 6HF \rightarrow H_2SiF_6 + 2H_2O$$

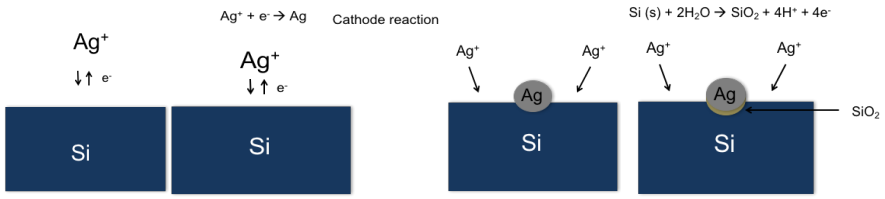

Figure 1 Procedure of Si nanowire synthesis [23,24]

A downside of metal-assisted chemical etching method is a roughened surface nanowires. However, this can be advantageous when used for thermoelectric applications due to increased phonon scattering which leads to reduced thermal conductivity as shown in previous studies [9]

Silicon nanowire synthesis procedure

Silicon nanowire synthesis in this experiment was conducted on p-type (100) silicon wafer with. The wafers were cut into small pieces (2 cm x 2 cm) and placed inside a glass beaker. With the addition of acetone, the cut wafers were sonicated for 5 minutes. The wafers are then rinsed with acetone, IPA and Millipore water and sonicated. The wafers were then dried with compressed air and the backside of the wafers were coated with nail polish and left to dry for 10 minutes. In separate polyethylene beakers 0.754g $AgNO_3$ was mixed with 225 mL Millipore water and 39 mL of HF. The $AgNO_3$/HF solution was then transferred to the beaker containing the wafers and the reaction mixture is left for 2 – 4 hours for nanowires to develop. The solution mixture was then decanted along with the silver dendrite cloud. The wafers were then rinsed with Millipore water and IPA following by drying with compressed air. To get rid of silver, the top can be rinsed away with water. Silver in the array was removed by immersing the wafers in nitric acid for 30 minutes. Finally, the wafers were rinsed with Millipore water and IPA then dried with compressed air.

Silicon nanowire characterization

Grown silicon nanowires are characterized using FEI Quanta^{TM} 3D FEG Duel Beam (SEM/FIB). the length of the nanowires were measured by imaging the cross-sectional view of the silicon chip as shown in Figure 2. The nanowires formed are mostly bundled.

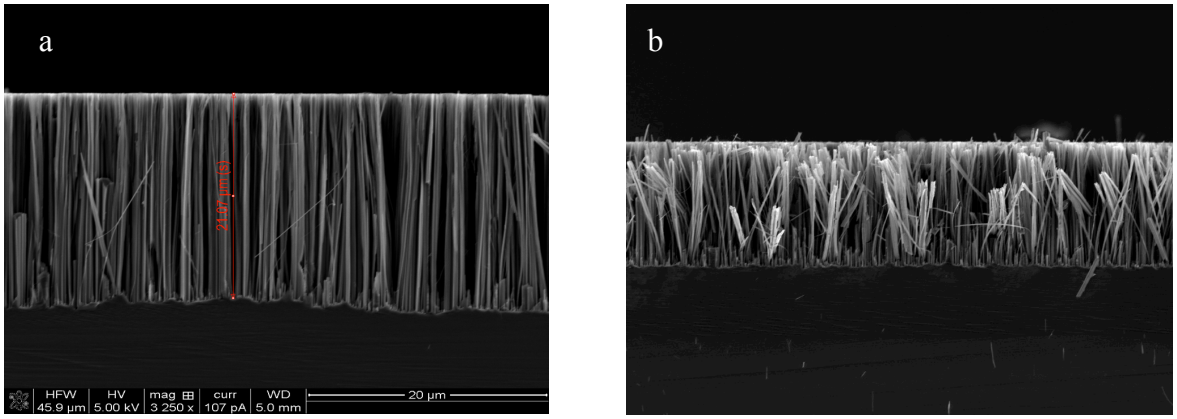

Figure 2 (a) cross-sectional view of Si chip the grown Si nanowires. The length of the grown wires is in the range of 21 μm. (b) cross-sectional view of Si chip showing grown nanowires in bundles**.**

Nanowire transfer procedure

The following step is to transfer an individual nanowire from the prepared silicon chip onto the microfabricated device. First, silicon nanowires chip is cut into a piece and added to a vial containing ethanol solution. The vial is then immersed in a sonication bath. This process leads to a solution in which nanowires are dispersed. Then, a drop cast of the nanowire solution over a TEM grid to have the nanowires scattered over the TEM surface to ease the manipulation process. A manipulator inside the SEM chamber is used to carry the nanowire and bond it onto the microfabricated device. Figure 3 shows the manipulation process. The nanowire is carried by the manipulator where it is mechanically and thermally anchored on the Pt electrode using electron beam induced deposition (EBID) of Pt inside the SEM chamber. Figure 4 shows the final stage where the nanowire is bridged between the heating and sensing membrane.

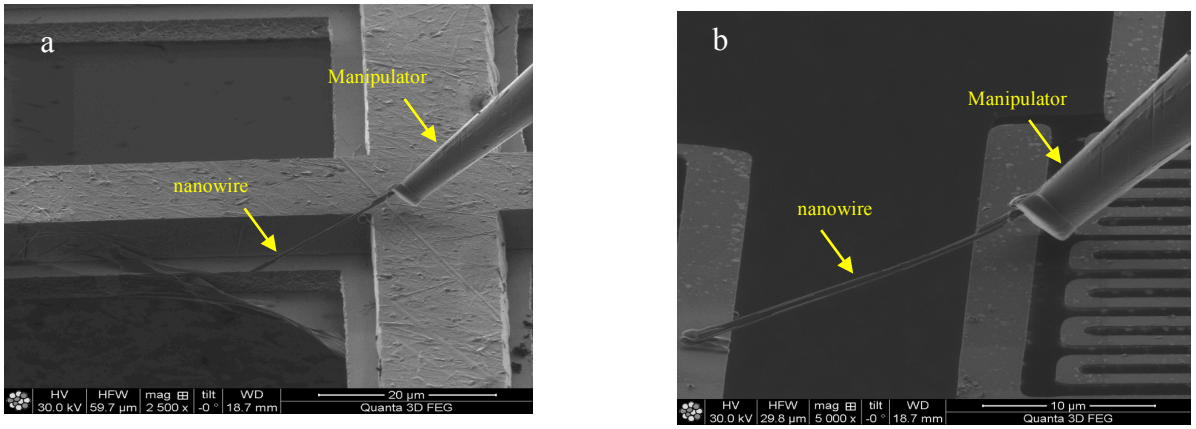

Figure 3 silicon nanowire manipulation inside the SEM chamber. The images are shown using Focused ion beam for illustration purposes (a) the nanowire is picked up from the end carry a nanowire on a TEM grid. Pt is deposited using Electron Beam Induced Deposition (EBID) to make a contact and attach the nanowire to the manipulator (b) placement of a nanowire to bridge the two membranes. The manipulator is pulled out mechanically to detach the nanowire after bonding one side to the membrane and another bond is made after detachment from the manipulator

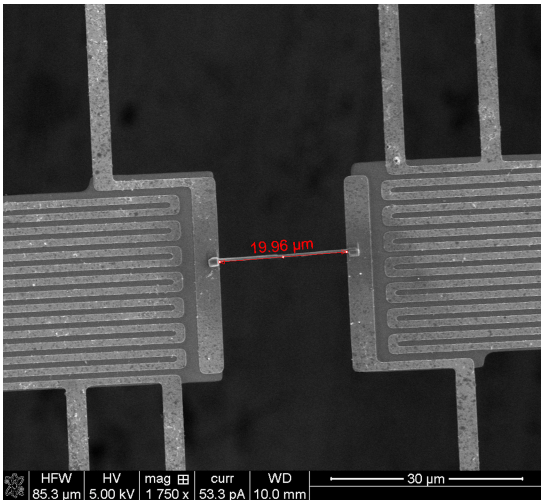

Figure 4 SEM image of the bridged nanowire between the membrane after Pt deposition.

After a successful transfer of a nanowire sample onto the suspended microdevice and making thermal contact, the device is mounted on a pin package and wire bonded to make an electrical contact between the pin package and the Pt pads on the microdevice. The pin package is then placed inside the cryostat chamber with vacuum level in the order of 10-6 Torr. The temperature of the chamber is controlled by Lakeshore 332 Temperature Controller. The cooling is controlled by SHI Cryogenics Group's Zephyr™ compressor (Model HC-4A1). The setup consists of a cryostat holding the pin package containing the microdevice and a temperature sensor positioned below the pin package. Lake Shore Cryogenic wires are used for electrical connections between the pin package and the electric connected to the equipment. The wires provide insulation with to ensure that no short circuit occur.

Chapter 3 Heat transfer analysis of the micro-device

The two suspended membranes are denoted as the heating and sensing membrane. The mechanism of thermal conductance measurement is shown in Figure 5. A DC current (I_{DC}) coupled with a small AC current (i_{ac}) passes through the platinum resistive thermometer (PRT) coil of the heating membrane. The AC current is used to measure the resistance of the heating PRT. Since i_{ac} is much smaller than I_{DC}, joule heating triggered by i_{ac} is negligible. Therefore, a joule heat $Q_h = I^2 R_h$ is generated due to flow of DC current in the heating PRT, where R_h is the resistance of the PRT. A lock-in amplifier (SR810 Stanford Research Systems) is used to measure the first harmonic component (v_{ac}) of the voltage drop across the two inner probes of the PRT. Part of the heat generated, a joule heat $2Q_L = 2I^2 R_L$ is dissipated in the two Pt beams that supply the DC current to the heating PRT yielding a parabolic temperature distribution along the two beams. A certain amount of heat, Q_2, is conducted through the nanowire sample from the heating to the sensing membrane, which cause a temperature rise T_s in the sensing membrane. The remaining heat is conducted through the other five beams that support the sensing membrane. The rest of the heat, $Q_1 = 2Q_L - Q_2$, is conducted through the five beams in the heating membrane. [5]

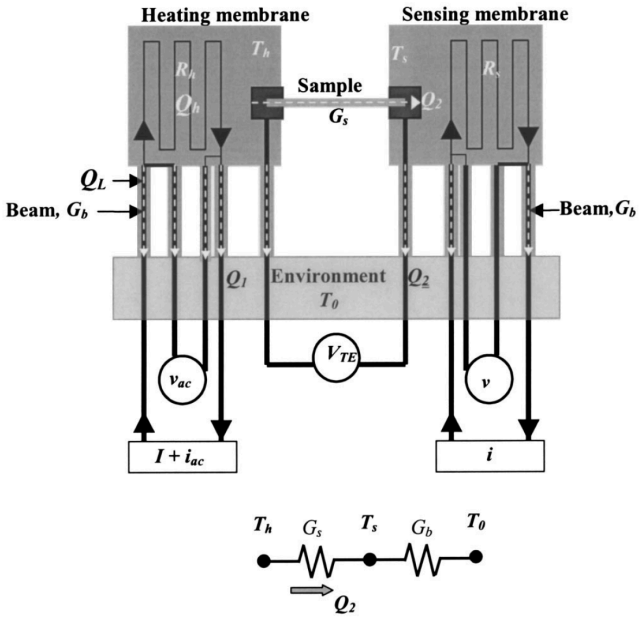

Figure 5 A schematic showing the mechanism of thermal conductance measurement of one-dimensional nanostructure

The five beams supporting each membrane are identically designed. The total thermal conductance of the five beams can be expressed as

$$G_b = 5\frac{k_b A}{L} \quad (17)$$

where k_b is the thermal conductivity, A is the cross-sectional area, and L is the length of each beam. Based on thermal resistance analysis in Figure 5, we can obtain the following equation

$$Q_2 = G_s(T_h - T_s) = G_b(T_s - T_0) \quad (18)$$

Similarly, for the heating membrane we can obtain the following expression

$$Q_1 = G_b(T_h - T_0) \quad (19)$$

The heat conduction to the environment from the two beams supplying the heating current can be expressed as $Q_{h,2} = 2\left(\frac{G_b\,\Delta T_h}{5} + \frac{Q_L}{2}\right)$; while the heat conduction to the environment from the remaining three beams of the heating membrane can be expressed as $Q_{h,3} = 3\frac{G_b\,\Delta T_h}{5}$. The heat conduction to the environment from the five beams connected to the sensing membrane can be expressed as $Q_{s,5} = G_b\,\Delta T_s$. Therefore, considering conservation of energy $Q_{h,2} + Q_{h,3} + Q_{s,5} = Q_h + 2Q_L$, we obtain expressions for the thermal conductance of the beams and the sample as follows:

$$G_b = \frac{Q_{tot}}{\Delta T_s + \Delta T_h} = \frac{Q_h + Q_L}{\Delta T_s + \Delta T_h} \quad (20)$$

$$G_s = G_b \frac{\Delta T_s}{\Delta T_h - \Delta T_s} \quad (21)$$

where G_s is the thermal conductance of the nanowire sample and consists of two components, namely, the intrinsic thermal conductance G_n and the contact thermal conductance G_c according to the equation $G_s = (G_n^{-1} + G_c^{-1})^{-1}$

To obtain an expression for the temperature rise of both the heating and sensing PRT, their resistance and their temperature coefficient of resistance (TCR) are measured, where $TCR = \frac{1}{R}\frac{dR}{dT}$. The TCR of both the heating and sensing PRT is extracted by measuring the resistances of the PRT as a function of temperature. We obtain $\frac{dR}{dT}$ from the local fit of the $R - T$ curve. The differential resistance ΔR_h, is obtained by measuring the $I - V$ of the heating PRT while ramping up the DC current. This gives the change in resistance of the PRT as joule heat is supplied. Similarly, the differential resistance of the sensing membrane is measured by measuring the $I - V$ of the sensing PRT. Hence, it can be shown that the temperature rise in both membranes can be expressed as follows

$$\Delta T_h = \frac{\Delta R_h}{R_h \times TCR} \quad (22)$$

$$\Delta T_s = \frac{\Delta R_s}{R_s \times TCR} \quad (23)$$

Chapter 4 Experimental Results

In this work, we have obtained thermal conductivity measurement results of the synthesized Si nanowires. The samples prepared were mainly bundled nanowires. Thus, the magnitude of the expected results is questionable due to inconsistency in diameter along the nanowire length and due to surface to surface contact between the nanowires. This chapter will show experimental measurements for three different samples with varying length and diameter. Figure 6a shows an illustration of current – voltage plot. The slope represents the initial resistance of the PRT without joule heating. Figure 6b shows the resistance as a function of temperature. The local slope is used to calculate the TCR for both membranes. Following the procedure detailed in Chapter 3, we measured the thermal conductivity of Si nanowires with diameters of 420 nm, 130 nm and 120 nm. The set of data is shown in Figure 7.

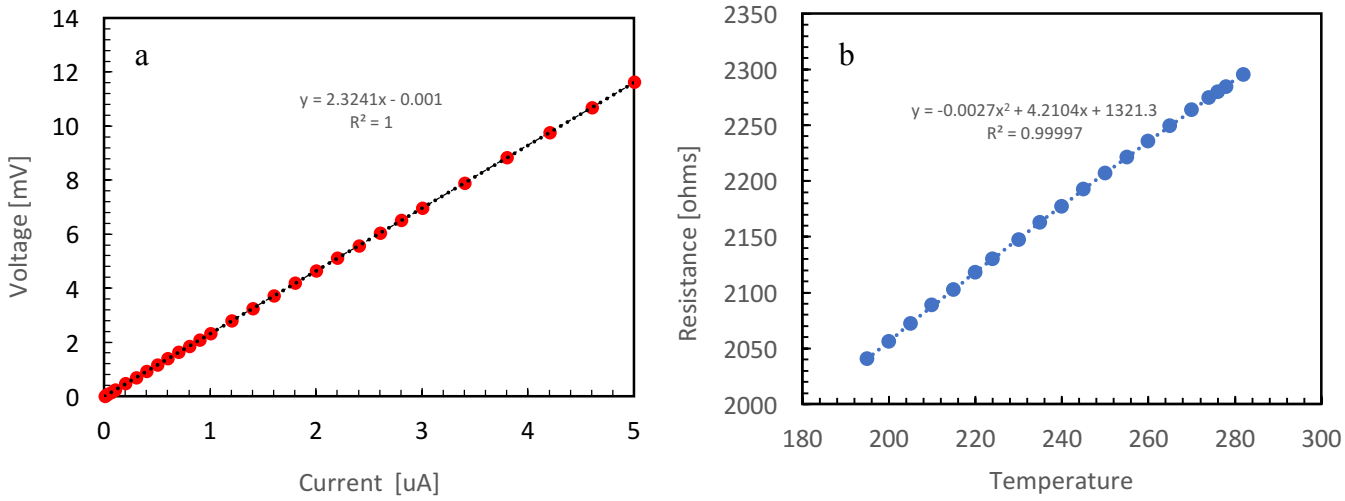

Figure 6 (a) $I-V$ plot for resistance measurements. (b) temperature dependent resistance measurement. The resistance is measured at variable temperatures where a local polynomial slope is taken to calculate the TCR of the resistive thermometer.

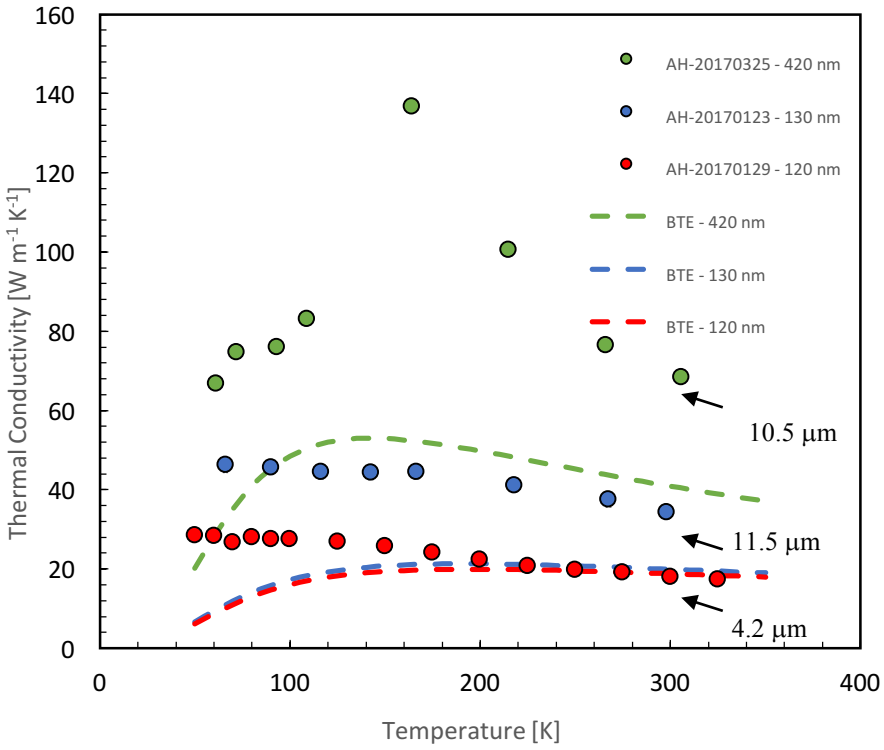

Figure 7 Thermal conductivity results obtained for three different samples. The green, blue and red correspond to silicon nanowires of diameters 420 nm, 130 nm, and 120 nm, respectively. The dashed lines are based on BTE model.

The results obtained for the thickest nanowire (420 nm) is not a reliable estimate since the diameter is very large, thus, we are dealing with a large characteristic length that is approaching the bulk. Also, thorough TCR measurements and further modifications must be taken into account for future measurements. Further analysis on contact resistance must also be investigated. To have a better approximation for contact resistance; length-dependent resistance measurements must be considered for future experiments. This will provide more accurate estimation of the intrinsic thermal conductivity of SiNWs. Additional measurement will be carried out for a new batch of synthesized Si nanowires.

Chapter 5 Analysis of Measurement Limits

Multiple experimental and computational studies have been conducted to quantify the thermal conductivity of 1D and 2D materials where it explored various high conductance and low conductance materials. On the high end spectrum of thermal conductivity, carbon based materials dominates the ladder due to their high group velocity in addition to shortage of processes that promote phonon scattering. [6]. Other high conductance materials were also investigated. Lindsay *et al*. reported thermal conductivity values for cubic III-V Boron based crystals such as Baron Arsenide ranging from 2000 W/mK which are comparable to carbon based materials such as diamond and graphite. [25]. Single-layer graphene values reported ranged from 2000 W/mK to 5500 W/mK at room temperature and down to 600 W/mK at 680 K. [12]. On the lower end of the spectrum, To evaluate the accuracy of the reported extreme high and low conductance results, quantifying measurement limits becomes inevitable due to the increase in contribution of radiation and contact resistance at the higher and lower bound limits of conductance. Previously, Cahill reviewed the limits of thermal conductivity at the extremes and the thermal conductance of multiple interfaces [6]. With the ongoing investigation of thermal properties of high and low conductance materials, the question that arise is, what are the measurement limits of conductance that can be attained experimentally in which the interference contact conductance and radiation heat exchange becomes considerably insignificant? To answer this question, we calculated the thermal conductance computationally to estimate the limits based on sample geometrical characteristic over a wide temperature range. We based our analysis on select high and low conductance materials.

In this study, we performed computational estimations for thermal conductance in the temperature range of 5 K up to 1000 K to quantify the conductance limits with respect to geometrical characteristics of common nanostructures. Figure 8 shows an illustration of the conductance limits for Si nanowire. The upper limit is bounded by conductance due to radiation heat exchange between the sample and the environment. The lower limit is bounded by the interfacial contact conductance. The thermal conductance due to radiative heat exchange for nanowires can be estimated as

$$G_{rad} = 4\varepsilon\sigma T^3 PL \qquad (24)$$

where ε is the emissivity of the nanowire, σ is the Stefan-Boltzmann constant, P is the perimeter of the nanowire and is proportional to $2\pi r$. To assume a worst case scenario in terms of measurement limitations we set the emissivity ε=1. [26]

Thermal conductivity measurement results can be underestimated when neglecting the thermal contact resistance of the interface. Thermal contact conductance has been investigated to quantify the upper limit of thermal conductance which tells us the limitations of sample measurements in terms of sample geometries that can be obtained without having a substantial contribution from contacts. In this study, thermal contact conductance of Pt-Si in the range of 5 K up to 1000 K has been analyzed computationally. Diffuse-Mismatch Model (DMM) has been used for our contact resistance analysis. Boundary resistance is measured according to

$$R_{b,1-2}(T) = \left(\frac{1}{12}\frac{\sum_i v_{2,i}^{-2}}{\sum_i v_{1,i}^{-2}+\sum_i v_{2,i}^{-2}}\sum_i v_{1,i}\right)^{-1} C_1(T)^{-1} \qquad (25)$$

Where $R_{b,1-2}$ is the boundary resistance at the interface of material 1 and 2,$v_{1,i}$, $v_{2,i}$ are the mode-dependent sound velocity for material 1 and 2, respectively. C_1 is the heat capacity of material 1 [27]

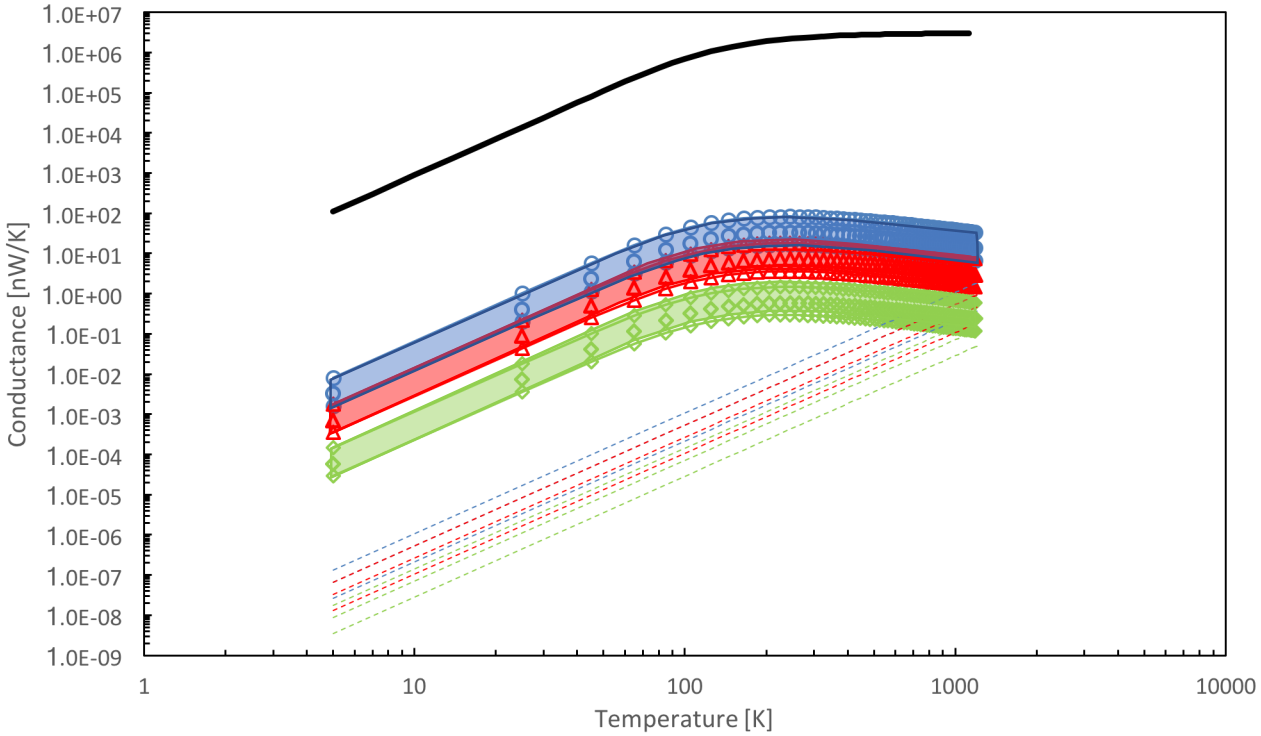

Figure 8 Logarithmic scale of conductance model of Si nanowire as a function of temperature based on BTE. This model illustrates temperature and length dependence for three different diameters. The diameters are represented by blue, red and green for 150 nm, 70 nm, and 20 nm, respectively. The shaded area represents the range of conductance by varying the length at constant diameter. The dashed lines represent the thermal conductance due to radiative heat exchange between the nanowire and the surrounding with varying length corresponding to different nanowire diameters. Contact conductance (black line) is modeled based on DMM.

Si Nanowires

Thermal transport in Si nanowires have been explored over a wide range by various researchers [4,7,9,10]. Thermal conductivity of smooth-surface Si nanowires have been studied by Li et al. [7] in which they demonstrated a size dependent thermal conductivity for nanowires in the range of 22 and 115 nm over a temperature range of 20-320 K. Later rough nanowires have had more attention due to their surface roughness effect which reduced the thermal conductivity substantially as illustrated by previous studies [9]. The thermal conductivity was shown to be as low as ~ 1.6 W/m K which is close to the amorphous limit of 1 W/m K for Si [28]. To quantify the upper conductance limit for low conductance Si nanowires, we have investigated the limits computationally utilizing BTE model to quantify the conductance upper limit for Si nanowires by investigating geometrical dependence over a wide temperature range. As shown in Figure 9, the thermal conductance of silicon nanowire 150 nm in diameter and 10 μm in length is three order of

magnitude higher than the corresponding G_{rad} at room temperature. This limit gap is further reduced to less than one order of magnitude at temperatures approaching 1000 K range. This tells us that for Si nanowires 150 nm in diameter and 10 μm in length, we can safely neglect the contribution of heat loss from the circumference of the sample unless the temperature exceeds ~ 950 K. As the diameter is reduced the contribution of radiation becomes substantially higher. for a 20 nm in diameter and 10 μm in length silicon nanowire the thermal conductance is within the same order of magnitude as G_{rad} at 965 K which is approximately ≈ 0.128 nW/K.

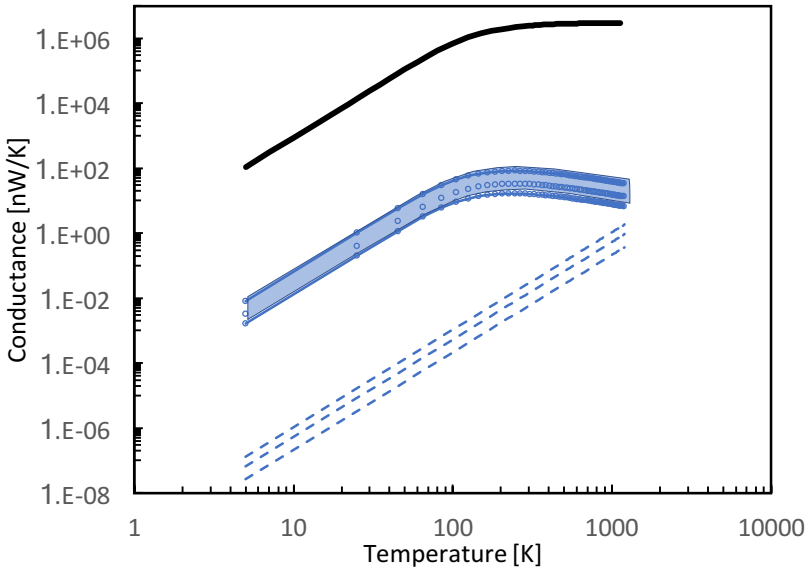

Figure 9 Log scale temperature dependent conductance model for a 150 nm Si nanowire based on BTE model. The lower limit of the conductance is bounded by conductance due to radiative heat exchange indicated by the dashed lines, each representing nanowire length (2 μm to 10 μm). The upper conductance limit is bounded by Pt-Si thermal contact conductance (black line).

To model the temperature dependent contact conductance, the thermal boundary conductance, G_b is obtained from the DMM approximation. The contact conductance can be extracted from the boundary resistance modeled data by defining the appropriate contact area. We estimate the contact area to be $A_c = 2\pi r L_c$ where r is the radius of the sample. The contact length (the length over which the contact metal covers a sample) is approximately $L_c \approx 2\ \mu m$. The estimated contact conductance of a 150 nm diameter Si nanowire is ~ G_c=2.5 x 10^6 nW/K at room temperature. Figure 9 shows the contact conductance in nW/K for a 150 nm diameter Si nanowire. This tells us the lower limit of conductance.

Si Thin Film

Previous studies on thermal transport in Si thin film both Computational [29], and experimental [30, 31] have been explored for size effect and temperature dependence. Goodson *et al* demonstrated a thermal conductivity reduction through size effect on Single-crystal silicon layers between 0.4 μm and 1.6 μm based on boundary scattering analysis [30]. Lie *et al* measured room

temperature thermal conductivity of 20 nm thick Si thin film of ~22 W/ mK, which is an order of magnitude smaller than the bulk value. Later, computational analysis explored the in-plane thermal conductivity in Si thin films over a large temperature range have been investigated as demonstrated by Huang et al. In this paper, similar analysis has been performed on Si thin film quantifying the conductance limits. Figure 10 shows a log scale temperature dependent conductance model. The conductance is modeled based on Callaway-BTE for Si thin film of thicknesses 10 nm up to 1 μm. We infer from the results that radiation contribution for thin films with thickness 100 nm and above is safely negligible even at extreme high temperatures. The concern is when the thickness reaches 10 nm or lower and the temperature range exceeds 965 K. this is based on a 30 μm long Si thin film.

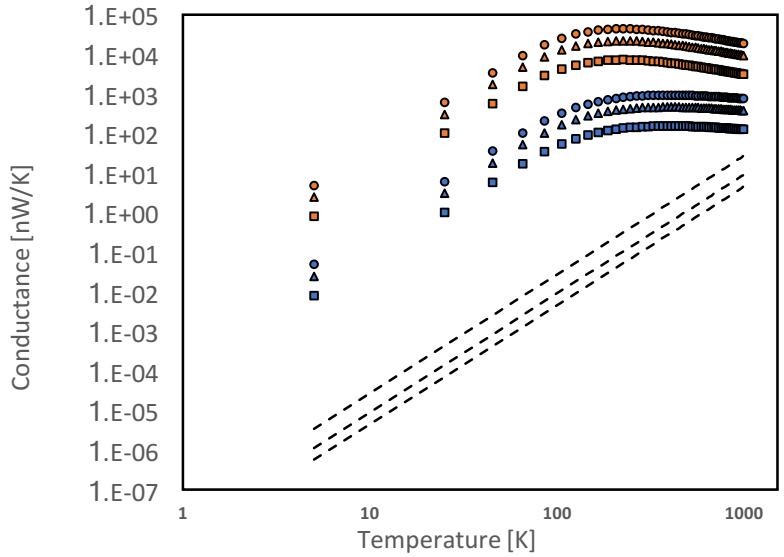

Figure 10 Logarithmic scale temperature dependent conductance model for Si thin film. The model is based on Callaway- BTE. The thin film thickness ranged from 10 nm to 1 μm for length from 5 μm up to 30 μm.

Carbon Nanotubes

Thermal conductivity of single-wall carbon nanotubes (CNT) has been investigated previously [11]. Pop, E. *et al* studied single-wall carbon nanotubes above room temperatures. They reported extracted values of thermal conductance for SWCNT at approximately $G \approx 2.4$ nW/K and $k \approx 3500$ W/mK at room temperature for $L \approx 2.6$ μm and $d \approx 1.7$ nm [11]. In our analysis, we quantified the lower limit of thermal conductance. To compute the thermal conductance of SW CNT, we based our analysis by employing the analytical approximation of thermal conductivity introduced previously [11]. The model captures the temperature dependent thermal conductivity of carbon nanotubes while taking into account contributions from Matthiessen's rule. Figure 11 shows that at temperatures below 10 K the contact conductance is only one order of magnitude higher than the sample conductance for a 2 μm carbon nanotube. The estimation is based on a 2 nm diameter sample. Due to the fact that the DMM underestimates the boundary resistance due to contribution of processing impurities [26], the contact conductance of the Pt-C interface overestimates the limits. Therefore, we expect to have a noticeably higher contributions of contact resistance to the measurements of carbon nanotubes within this temperature range.

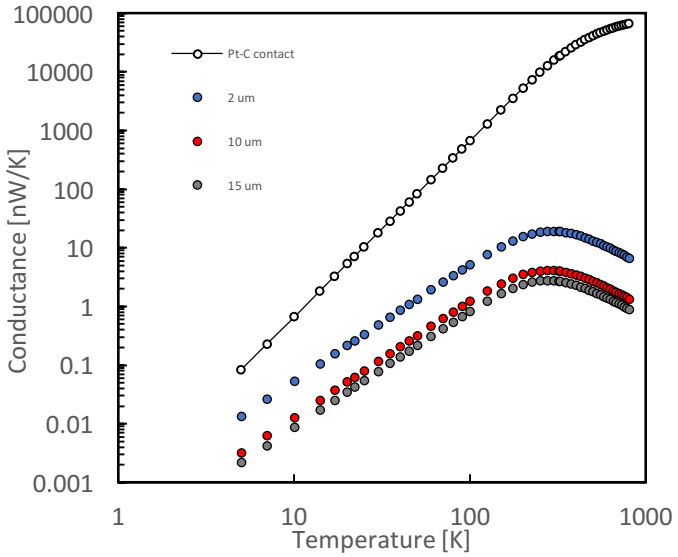

Figure 11 Analytical temperature dependent conductance of single-walled carbon nanotubes (SWCNT) in the range of 5 K to 800 K for 2 nm constant diameter and at different lengths. Thermal conductance was calculated based on the analytical model for thermal conductivity for SWCNT. Pt-C contact conductance data are extracted from the boundary resistance modeled based on heat capacity dependence – DMM

Conclusion

In this work, we have demonstrated experimental thermal conductivity measurement of Si nanowires synthesized through metal-assisted chemical etching. Our results indicate that further experiments shall be conducted for multiple nanowire devices in the future. In this work, we also studied the thermal conductance measurement limits based on the analysis of radiation heat exchange and boundary resistance to quantify the limits in which the contribution of radiation and contact conductance are negligible relative to the measured conductance. The computations were done studying common nanostructures, including Si nanowires, Si thin film, and single-wall carbon nanotubes. can set a guideline for a limit of diameter and length in which the contribution of conductance due to radiation and contact resistance

References

[1] J. Fourier, Théorie Analytique de la Chaleur [The Analytic Theory of Heat], Firmin Didot Père et Fils, Paris, 1822

[2] Tien CL, Chen GG. Challenges in Microscale Conductive and Radiative Heat Transfer. ASME. J. Heat Transfer. 1994;116(4):799-807.

[3] Rojo, Miguel Muñoz et al. "Review on Measurement Techniques of Transport Properties of Nanowires Additions and Corrections. ." *Nanoscale* 5.23 (2013): 11526–11544. *PMC*. Web. 4 June 2017.

[4] A. I. Boukai, Y. Bunimovich, J. Tahir-Kheli, J.-K. Yu, W. A. Goddard, and J. R. Heath, "Silicon nanowires as efficient thermoelectric materials.," *Nature*, vol. 451, no. 7175, pp. 168–71, 2008

[5] L. Shi *et al*., "Measuring thermal and thermoelectric properties of one-dimensional nanostructures using a microfabricated device," *J.\ Heat Transf.*, vol. 125, no. 5, pp. 881–888, 2003.

[6] D. G. Cahill, "Extremes of heat conduction—Pushing the boundaries of the thermal conductivity of materials," *MRS Bull.*, vol. 37, no. September, pp. 855–863, 2012.

[7] Li, D.; Wu, Y.; Kim, P.; Shi, L.; Yang, P.; Majumdar, A. Thermal Conductivity of Individual Silicon Nanowires. Appl. Phys. Lett. 2003,83, 2934-2936

[8] A. Mavrokefalos, A. L. Moore, M. T. Pettes, L. Shi, W. Wang, and X. Li, "Thermoelectric and structural characterizations of individual electrodeposited bismuth telluride nanowires," *J. Appl. Phys.*, vol. 105, no. 10, p. 104318, May 2009.

[9] Hochbaum, A. I.; Chen, R.; Delgado, R. D.; Liang, W.; Garnett, E.C.; Najarian, M.; Majumdar, A.; Yang, P. "Enhanced Thermoelectric Performance of Rough Silicon Nanowires". Nature 2008, 451, 163-167

[10] Chen, R.; Hochbaum, A. I.; Murphy, P.; Moore, J.; Yang, P., Majumdar, A., "Thermal conductance of thin silicon nanowires."*Phys. Rev. Lett.* **2008**, *101* (10), 14.

[11] E. Pop, D. Mann, Q. Wang, K. Goodson, and H. Dai, "Thermal Conductance of an Individual Single-Wall Carbon Nanotube above Room Temperature," , Nano Lett, 2006.

[12] X. Gu and R. Yang, "Phonon transport and thermal conductivity in two-dimensional materials," *arXiv*, pp. 1–67, 2015.

[13] Callaway, J.: Model for lattice thermal conductivity at low temperatures. Phys. Rev. 113, 1046–1051 (1959)

[14]. Holland, M.G.: Analysis of lattice thermal conductivity. Phys. Rev. 132, 2461–2471 (1963)

[15]. Mingo, N.: Calculation of Si nanowire thermal conductivity using complete phonon dispersion relations. Phys. Rev. B 68, 113308 (2003)

[16]. McConnell, A.D., Goodson, K.E.: Thermal conduction in silicon micro- and nanostructures. Ann. Rev. Heat Tran. 14, 129–168 (2005)

[17] Dames, C., Chen, G.: In: Rowe, D.M. (ed.) Thermo- electrics Handbook, Macro to Nano. Taylor & Francis, New York (2006)

[18] Lee, J. In *Encyclopedia of Nanotechnology*; Bhushan, B., Ed.; Springer Netherlands: Dordrecht, 2016; pp 1453–1462.

[19] Volz, S. G., and Chen, G., 1999, ''Molecular Dynamics Simulation of Thermal Conductivity of Silicon Nanowires,'' Appl. Phys. Lett., 75, pp. 2056–2058.

[20] Khitun, A., Balandin, A., and Wang, K. L., 1999, ''Modification of the Thermal Conductivity in Silicon Quantum Wires Due to Spatial Confinement of Acoustic Phonons,'' Superlattices Microstruct., 26, pp. 181–193.

[21] P. E. Hopkins *et al*., "Reduction in the Thermal Conductivity of Single Crystalline Silicon by Phononic Crystal Patterning," pp. 107–112, 2011.

[22] K. Peng, J. Hu, Y. Yan, Y. Wu, H. Fang, Y. Xu, et al., "Fabrication of Single-Crystalline Silicon Nanowires by Scratching a Silicon Surface with Catalytic Metal Particles,"Advanced Functional Materials, vol. 16, pp. 387-394, 2006

[23] Z. Huang, N. Geyer, P. Werner, J. De Boor, and U. Gösele, "Metal-Assisted Chemical Etching of Silicon: A Review," Advanced materials, vol. 23, pp. 285-308, 2011.

[24] R. Wagner and W. Ellis, "Vapor-liquid-solid mechanism of single crystal growth," Applied Physics Letters, vol. 4, pp. 89-90, 1964.

[25] L. Lindsay, D. A. Broido, and T. L. Reinecke , "First-Principles Determination of Ultrahigh Thermal Conductivity of Boron Arsenide: A Competitor for Diamond?", Phys. Rev. Lett. **111**, 025901 – Published 8 July 2013

[26] J. Lee *et al*., "Thermal Transport in Silicon Nanowires at High Temperature up to 700 K," *Nano Lett*., vol. 16, no. 7, pp. 4133–4140, 2016.

[27] Bellis, L. De, Phelan, P. E. & Prasher, R. S. "Variations of Acoustic and Diffuse Mismatch Models in Predicting Thermal-Boundary Resistance". J. Thermophys. Heat Transf. 14, 144 150 (2000).

[28] Cahill, D. G.; Watson, S. K.; Pohl, R. O. “Lower Limit to the Thermal Conductivity of Disordered Crystals”. Phys. Rev. B: Condens. Matter Mater. Phys. 1992, 46, 6131–6140

[29] X. Wang and B. Huang, “Computational study of in-plane phonon transport in Si thin films.,” *Sci. Rep.*, vol. 4, p. 6399, 2014.

[30] Asheghi, M., Leung, Y.K., Wong, S.S., and Goodson, K.E., 1997, "Phonon-Boundary Scattering in Thin Silicon Layers," *Applied Physics Letters*, Vol. 71, pp. 1798-1800.

[31] W. Liu and M. Asheghi, “Phonon – boundary scattering in ultrathin single-crystal silicon layers,” Applied Physics Letters, vol. 3819, no. 2004, pp. 2002–2005, 2005.